Evaluation of Total Cloudiness and Its Variability in the Atmospheric Model Intercomparison Project

BRYAN C. WEARE,* IGOR I. MOKHOV,** AND PROJECT MEMBERS@

* *Atmospheric Science Program, University of California, Davis, California*
** *Institute of Atmospheric Physics, Russian Academy of Sciences—Moscow*

(Manuscript received 14 September 1994, in final form 13 March 1995)

ABSTRACT

Total cloudiness of 29 models participating in the Atmospheric Model Intercomparison Project is compared with the ISCCP C2 as well as the *Nimbus-7* and Meteor observational estimates. The root-mean-square differences between the annual means of the model calculations and the C2 observations after global means are removed vary from about twice to nearly four times the difference between the C2 and Meteor observations. The large differences are in some cases due to the fact that although a model qualitatively has patterns of spatial variations similar to those of the observations, the magnitude of those variations is much too small. In other cases the models have produced the approximate magnitude of the spatial variability of the observations but display sizable errors in the pattern of that variability.

Deficiencies with respect to the model simulations of the mean seasonal cycle are also pronounced. For instance, the differences between the zonal averages of total cloudiness for contrasting seasons suggest that near 60° most models predict minima in cloudiness in summer, whereas observations strongly suggest the opposite. In addition, smoothed seasonal cycle analyses suggest that a portion of these deficiencies in some models is the result of a simulated seasonal cycle that leads that of the observations by about two months. However, some models, which appear to have the proper phase of the seasonal cycle, still show large root-mean-squared differences and small correlations when compared with the smoothed seasonal cycle of the C2 observations. The C2 and Meteor observations show a modest signal in total cloudiness for the only important interannual variation during the July 1983 through June 1988 observation period—the 1986/87 ENSO event. A few models reproduce this event about as well as do the Meteor observations, whereas many models fail to show any evidence of it.

Overall, models that better reproduce the ENSO results also tend to do well with seasonal variations. No specific differences are evident in the physical characteristics of models that are relatively adept at reproducing seasonal and interannual variations and those that perform more poorly. However, there is the general conclusion that models that have more sophisticated physical processes tend to better simulate the cloud observations.

@ Project Members

Michael Blackburn,[a] George Boer,[b] David Burridge,[c] K. Campana,[d] Michel Déqué,[e] Valentin Dymnikov,[f] Wesley Ebisusaki,[d] Laura Ferranti,[c] Laura Fowler,[g] Vener Galin,[f] Christopher Hall,[h] Timothy Hogan,[i] Barrie Hunt,[j] Toshiki Iwasaki,[k] William K-M Lau,[l] Eugenia Kalnay,[d] Jeong-Woo Kim,[m] Akio Kitoh,[n] Hervé Le Treut,[o] Xin-Zhong Liang,[p] Kenneth Lo,[q] Jean-Francois Mahfouf,[e] Valentin Maleshko,[r] Bryant McAvaney,[s] Norman McFarlane,[b] Carlos Mechoso,[t] Kiku Miyakoda,[u] Jai-Ho Oh,[v] Chung-Kyu Park,[w] David Randall,[f] Erich Roeckner,[x] Richard Rood,[w] Thomas Rosmond,[i] Nobuo Sato,[k] Ulrich Schlese,[x] Michael Schlesinger,[y] Julia Slingo,[a] William Stern,[u] David Straus,[z] Tatsushi Tokioka,[n] Tadashi Tsuyuki,[k] Huug van den Dool,[d] Wei-Chyung Wang,[p] Richard Wetherald,[aa] David Williamson,[bb] and Qing-cun Zeng[cc]

Corresponding author address: Dr. Bryan C. Weare, Atmospheric Science, University of California-Davis, Hoagland Hall, Davis, CA 95616-8627.

[a] *UK Universities Global Atmosphere Modelling Programme, University of Reading, Reading, England;* [b]*Canadian Climate Centre, Victoria, BC, Canada;* [c]*European Centre for Medium-range Weather Forecasting, Reading, England;* [d]*National Meteorological Center, Camp Springs, MD, USA;* [e]*Centre National de Recherches Météorologiques, Toulouse, France;* [f]*Department of Numerical Mathematics, Russian Acad. of Science, Moscow, Russia;* [g]*Colorado State University, Fort Collins, CO, USA;* [h]*United Kingdom Meteorological Office, Bracknell, Berkshire, England;* [i]*Naval Research Laboratory, Monterey, CA, USA;* [j]*Commonwealth Scientific and Industrial Research Organization, Mordialloc, Victoria, Australia;* [k]*Japan Meteorological Agency, Tokyo, Japan;* [l]*Goddard Laboratory for Atmospheres, Goddard Space Flight Center, Greenbelt, MD, USA;* [m]*Yonsei University, Seoul, Korea;* [n]*Meteorological Research Institute, Tsukuba-shi, Japan;* [o]*Laboratorie de Météorologie Dynamique, Ecole Normale Superieure, Paris, France;* [p]*State University of New York at Albany, Albany, NY, USA;* [q]*Goddard Institute for Space Studies, New York, NY, USA;* [r]*Main Geophysical Observatory, St. Petersburg, Russia;* [s]*Bureau of Meteorology Research Centre, Melbourne, Victoria, Australia;* [t]*University of California-Los Angeles, Los Angeles, CA, USA;* [u]*Dynamical Extended Range Forecasting, GFDL, Princeton, NJ, USA;* [v]*Yonsei University, Seoul, Korea;* [w]*Goddard Space Flight Center, Greenbelt, MD, USA;* [x]*Max Planck Institute for Meteorology, Hamburg, Germany;* [y]*University of Illinois, Urbana-Champaign, Urbana, IL, USA;* [z]*Center for Ocean-Land-Atmosphere Studies, Calverton, MD, USA;* [aa]*Geophysical Fluid Dynamics Laboratory, Princeton, NJ, USA;* [bb]*National Center for Atmospheric Research, Boulder, CO, USA;* [cc]*Institute of Atmospheric Physics, Chinese Academy of Science, Beijing, China*

1. Introduction

The Intergovernmental Panel on Climate Change (Houghton et al. 1990, 1992) has emphasized that one of the key areas of uncertainty concerning the prediction of global climate properties is our incomplete understanding of the mechanisms involving the formation, dissipation, and radiative properties of cloud. Climate models form cloud in conjunction with two or sometimes three mechanisms. The simplest is related to large-scale saturation, which may be explicitly represented with prognostic cloud water variables or may be diagnosed such that a cloud is said to exist in a layer if the relative humidity exceeds a critical value. In many earlier models the grid was assumed to be either fully clouded or fully clear; more recent parameterizations allow for estimates of cloud fractions (Sundqvist 1988). The second mechanism for forming precipitating clouds is through one of the many parameterizations of cumulus convection. Again earlier parameterizations assumed that a grid square is either fully clouded or fully clear. Recently, empirical equations have been invoked to allow for varying partial cloudiness (Tiedtke 1988). The third form of cloudiness, which is only sometimes explicitly parameterized in general circulation models, is boundary-layer cloudiness. Until recently these clouds have almost always covered a full grid layer. Currently, empirical approaches to model fractional cloudiness are being attempted (Sommeria 1988).

The total cloudiness of 29 global climate models, run under the auspices of the Atmospheric Intercomparison Project (AMIP), has been compared to observations derived from the International Satellite Cloud Climatology Project (ISCCP) C2 (Rossow and Schiffer 1991). Observations derived from the *Nimbus-7* Cloud Analysis (N7) (Stowe et al. 1988) and the Russian Meteor series (Mokhov and Schlesinger 1993) are also used for comparison.

In order to effectively carry out model evaluations of total cloud amount, it must be fully recognized that the observations themselves are subject to considerable uncertainties arising from the imprecise nature of the definition of cloud amount and differing methods for cloud determination. Some authors (e.g., Ramanathan et al. 1989) have suggested that these difficulties dictate the use of "cloud radiative forcing" to evaluate the influences of clouds in observations and models. However, since the calculation of cloud radiative forcing in models requires the prior specification of cloud amounts as outlined above, we believe it is invaluable to compare cloud amounts in models with the best available observations. Nevertheless, the uncertainties force us to develop statistical measures of comparison that attempt to remove as much of the observational uncertainty as possible. For instance, since there is considerable disagreement concerning the exact magnitude of globally averaged cloud cover (Mokhov and Schlesinger 1994), this study will concentrate on comparing cloudiness differences after a global, annual, monthly, or regional mean has been removed. Our foremost conviction is that to be considered realistic in terms of total cloudiness a model must accurately portray the large-scale space–time variations that are common to the observations.

2. Models and data

Recently, AMIP has been thoroughly described by Gates (1992). Under the auspices of this project nearly all of the world's global atmospheric climate models have been run for a 10-yr period, with lower boundary conditions of sea surface temperatures (SST) and sea ice observed during the period January 1979 through December 1988. As the model runs are completed, the staff of the Program for Climate Model Diagnosis and Intercomparison (PCMDI) at the Lawrence Livermore National Laboratory transforms specified monthly statistics and daily model histories to standard formats and subjects them to quality control checks. Presently, only the monthly statistics are available for a large number of models. These monthly statistics include two measures of cloudiness: monthly mean total cloud cover for each model grid and monthly mean zonally averaged cloud fraction for each model latitude and pressure level. Only the former will be discussed in this paper.

In order to facilitate direct intercomparisons and comparisons with observations, all of the model total cloud values are interpolated to a common 5° latitude–longitude grid using a scheme provided by PCMDI. In the cases of models whose fundamental horizontal finite differencing is in terms of spherical harmonics, this interpolation was calculated from the model grid values derived by the modeling groups themselves. Sample maps of the 5° total cloudiness estimates were compared with those derived from the original model coordinates and were found to be in excellent agreement after accounting for the fact that some of the models have resolutions that are about twice that of the final 5°. Table 1, using information included in Phillips (1994), shows the names of the modeling groups whose models are analyzed here, their addresses, the abbreviations used throughout this paper, the horizontal and vertical resolution of the model, an indicator of the moist convection scheme used in the model, an indicator of how the convective cloud fraction is determined, and an indicator of how the stratiform cloud fraction is determined. Details of these latter indicators are found in Phillips (1994) and the many references included therein.

The ISCCP C2 summaries are currently available for July 1983 through December 1991. The ISCCP cloud data have been chosen as the primary comparison variable because we believe that they provide the best available multiyear global cloud analyses. The

TABLE 1.

Modeling group or observation set	Address	Abbreviation	Resolution[a]	Convection[b]	Convective cloud fraction[c]	Stratiform cloud fraction[d]
International Satellite Cloud Climatology Project		C2	2.5° × 2.5°			
Nimbus-7 Cloud Project		N7	4.5° × 4.5°			
Meteor		Meteor	5° × 5°			
Bureau of Meteorology Research Centre	Melbourne, Australia	BMRC	R31L9	Kuo, Tiedtke	Q(RH)	Q(RH)
Canadian Climate Centre	Victoria, Canada	CCC	T32L10	MCA	Q(RH)	L(RH)
Centre National de Recherches Météorologiques	Toulouse, France	CNRM	T42L30	Bough, Gel	L(precipitation)	Q(RH), 50% max.
Center for Ocean–Land–Atmosphere Studies	Calverton, Maryland	COLA	R40L18	Kuo, Tiedtke	F(precipitation)	Q(RH)
Commonwealth Scientific and Industrial Research Organization	Mordialloc, Australia	CSIRO	R21L9	AS, Gel	fixed	Q(RH), 50–70% max.
Colorado State University	Fort Collins, Colorado	CSU	4° × 5° L17	AS, MCA	100% if convection	100%, RH > threshold
Dynamical Extended Range Forecasting	Geophysical Fluid Dynamics Laboratory, Princeton, New Jersey	DERF	T42L18	MCA, Tiedtke	L(precipitation)	L(RH)
Department of Numerical Mathematics	Moscow, Russia	DNM	4° × 5°L 7	Kuo	Smag	Smag
European Centre for Medium-Range Weather Forecasting	Reading, England	ECMWF	T42L19	Tiedtke	F(precipitation)	Q(RH)
Geophysical Fluid Dynamics Laboratory	Princeton, New Jersey	GFDL	R30L14	MCA	100% if convection	100%, RH > threshold
Goddard Institute for Space Studies	New York, New York	GISS	4° × 5° L9	DGY	F(convection)	prognostic CW
Goddard Laboratory for Atmospheres	Greenbelt, Maryland	GLA	4° × 5° L17	AS	conical anvils	80%, RH > threshold
Goddard Space Flight Center	Greenbelt, Maryland	GSFC	4° × 5° L20	AS	F(AS)	100%, RH > threshold
Institute of Atmospheric Physics	Beijing, China	IAP	4° × 5° L2	AS	100% if convection	100%, RH > threshold
Japan Meteorological Agency	Tokyo, Japan	JMA	T42L21	Kuo, Tiedtke	100% if convection	Q(RH)
Laboratorie de Météorologie Dynamique	Paris, France	LMD	3.6° × 5.6° L11	MCA, Kuo	F(convection)	prognostic CW
Main Geophysical Observatory	St. Petersburg, Russia	MGO	T30L14	Kuo, MCA	F(precipitation)	Q(RH)
Max Planck Institute for Meteorology	Hamburg, Germany	MPI	T42L19	Tiedtke	prognostic CW	prognostic CW
Meteorological Research Institute	Ibaraki-ken, Japan	MRI	4° × 5° L15	AS, MCA	fixed	100%, RH > threshold
National Center for Atmospheric Research	Boulder, Colorado	NCAR	T42L18	Hack	20% < F(precipitation) < 80%	f(RH, —, precipitation)
National Meteorological Center	Camp Springs, Maryland	NMC	T40L18	Kuo	F(precipitation)	Q(RH)
Naval Research Laboratory	Monterey, California	NRL	T47L18	AS, Tiedtke	F(convection)	Q(RH)
State University of New York at Albany	Albany, New York	SUNYA	R15L12	MCA	F(convection)	95%, RH > threshold
State University of New York at Albany/NCAR	Albany, New York; Boulder, Colorado	SUNYANC	T31L18	KP	F(precipitation)	Q(RH)
University of California, Los Angeles	Los Angeles, California	UCLA	4° × 5° L15	AS	100% if convection	100%, RH > threshold
UK Universities Global Atmosphere Modelling Programme	Reading, England	UGAMP	T42L19	BM	F(precipitation)	Q(RH)
University of Illinois, Urbana—Champaign	Urbana, Illinois	UIUC	4° × 5° L7	AS, MCA	F(RH, convection)	prognostic CW
United Kingdom Meteorological Office	Bracknell, England	UKMO	2.5° × 3.75° L20	GR	F(precipitation)	prognostic CW
Yonsei University	Seoul, Korea	YON	4° × 5° L5	AS	F(convection)	Q(RH)

[a] Spherical harmonic truncations: R—rhomboidal, T—triangular, L—levels.

[b] Largely following the work of Arakawa and Schubert (1974), Betts and Miller (1993), Bougeault (1985), Del Genio and Yao (1988), Geleyn (1987), Gregory and Rowntree (1990), Hack (1994), Kreitzberg and Perky (1976), Kuo (1974), MCA-Manabe (1965), Tiedtke (1988).

[c] Treatment of convective clouds: L(precipitation)—linear function of precipitation rate, Smagorinsky (1960); Q(RH)—quadratic function of relative humidity; F(precipitation, convection, RH)—functions of convective precipitation, convective mass flux, or relative humidity; conical anvils—amount proportional to anvil size.

[d] Treatment of stratiform clouds generally following: Q(RH)—quadratic function of relative humidity, usually following Slingo (1987); L(RH)—linear function relative humidity; prognostic CW—prognostic cloud water with empirical cloud fraction; f(RH, —, precipitation)—function of relative humidity, vertical velocity, stability, and precipitation rate; xx%, RH > threshold—cloud fraction fixed at xx% if RH exceeds a threshold.

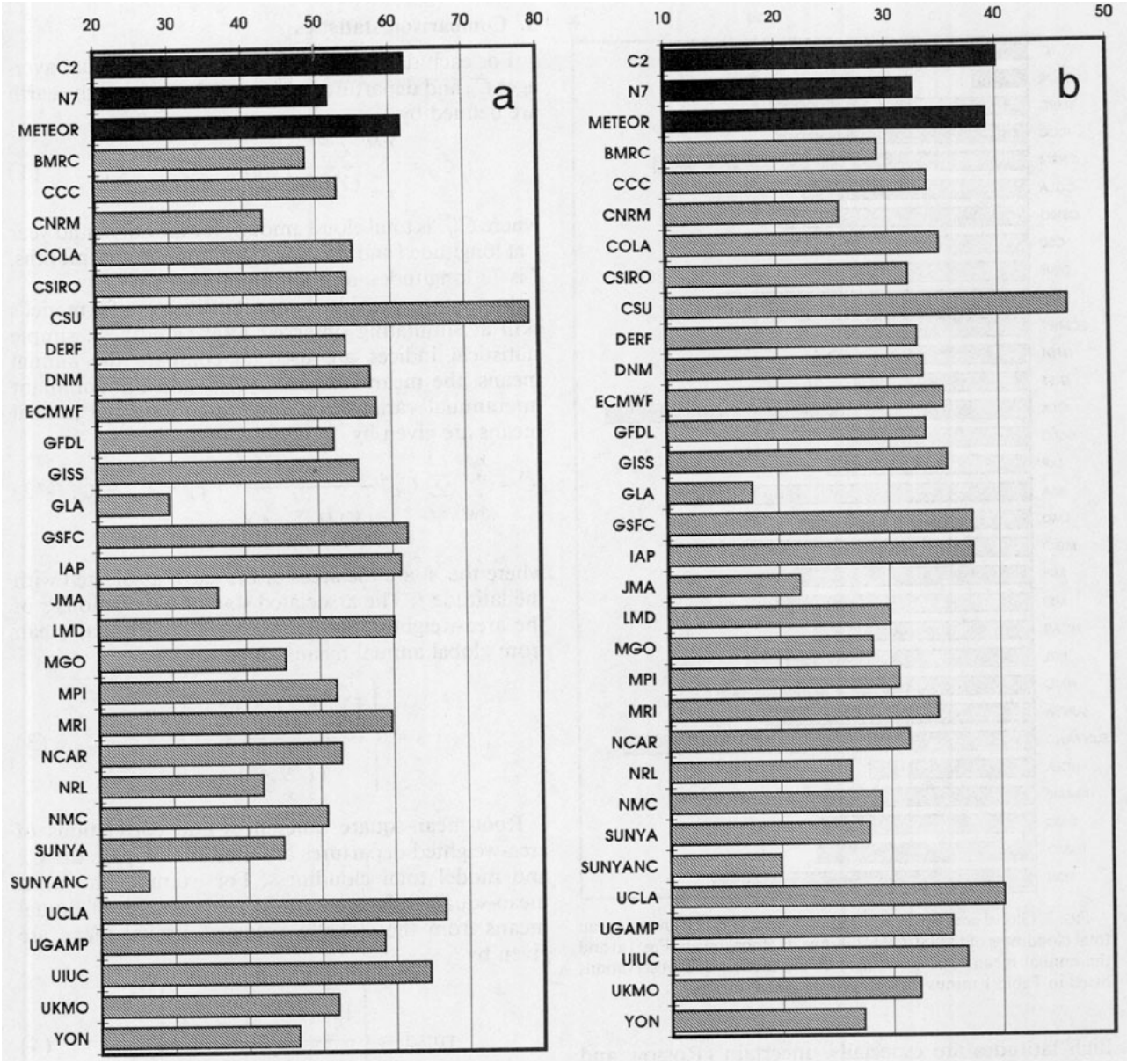

FIG. 1. Statistics of global area-weighted annual mean total cloudiness for the observed and model total cloud cover: (a) means and (b) standard deviations.

quality of these data is suggested by a number of studies. For instance, recent reports provide substantial evidence that ISCCP C2 monthly mean total cloud amounts statistics are in good general agreement with those of surface observations (Weare 1993; Mokhov and Schlesinger 1994) and those derived from analysis of multichannel high-resolution satellite observations (Weare 1992a). In addition, Weare (1993) shows that there are strong similarities between the intraannual correlations of ISCCP and the Consolidated Ocean Atmosphere Data Set (COADS) cloud amounts and sea surface temperature. Furthermore, Rossow and Schiffer (1991), Fu et al. (1991), and Weare (1993) support the contention that other ISCCP variables such as visible optical depth and cloud-top pressure at least qualitatively mimic important aspects of large-scale monthly averages. For example, Weare (1994) shows the intraannual correlations between COADS sea surface temperature and variations in ISCCP C2 cloud cover, cloud-top pressure, and vertically integrated cloud water content for the five years, July 1983–June 1988. In all three cases there are significant correlations over much of the World Ocean north of 40°S, the domain of sufficient COADS sampling. All satellite cloud variables over land have been judged to be less certain than those over ocean, and all observations at very

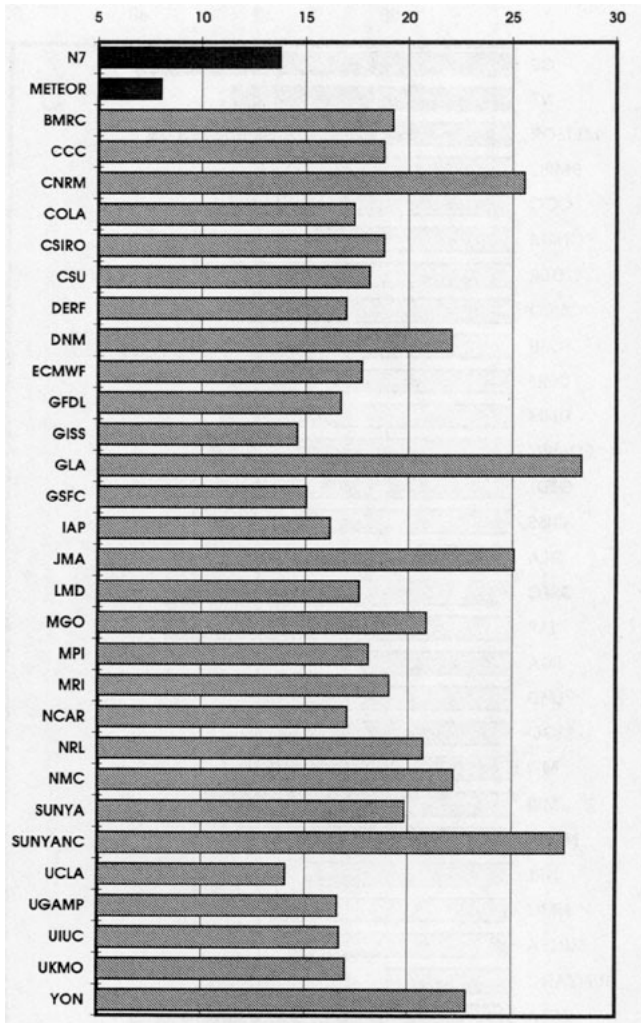

FIG. 2. Global area-weighted rmsd in percent between annual mean total cloudiness of the ISCCP C2 minus its global mean (Fig. 1a) and the annual mean total cloudiness of the models and observations listed in Table 1 minus their respective global means.

high latitudes are especially uncertain (Rossow and Schiffer 1991). The annual averages and departures used in this work are based upon the C2 period July 1983 through June 1988.

The *Nimbus-7* cloud data, which cover the period April 1979 through March 1985, are described in Stowe et al. (1988). They are derived from threshold tests using infrared and ultraviolet radiances and are available in an equal area grid with a resolution of approximately $(500)^2$ km^2. Weare (1992b) and Mokhov and Schlesinger (1993, 1994) have shown that the spatial patterns of these data compare favorably with surface estimates. Monthly mean Meteor total cloud estimates on a 5° × 5° latitude–longitude grid are available since 1979. These data are derived from coarse-resolution threshold tests (Mokhov and Schlesinger 1993). Both of these were transformed to the common 5° × 5° used in this study.

3. Comparison statistics

For each dataset or model output the annual averages $\bar{C}_{ij}$ and departures c_{ij}^{ym} for each point on the earth are defined by

$$\bar{C}_{ij} = \sum_{y,m}^{Y,M} \frac{C_{ij}^{ym}}{(YM)}; \quad c_{ij}^{ym} = C_{ij}^{ym} - \bar{C}_{ij}, \tag{1}$$

where C_{ij}^{ym} is total cloud amount for month m and year y at longitude i and latitude j: Y is 5 yr, M is 12 months, I is 72 longitudes, and J is 36 latitudes.

In order to provide compact estimates of a model's skill at simulating observed total cloudiness, simple statistical indices are used to compare the annual means, the mean seasonal cycles, and the dominant interannual variations. Global area-weighted annual means are given by

$$\bar{C} = \sum_{y,m}^{Y,M} \sum_{i,j}^{I,J} C_{ij}^{ym} \frac{A_j}{(YMI \sum_{j=1}^{J} A_j)}; \quad \bar{c}_{ij} = \bar{C}_{ij} - \bar{C}, \tag{2}$$

where the A_j are the areas of the earth associated with the latitude j. The associated standard deviations s of the area-weighted departures from the annual mean from global annual means are given by

$$s = \left\{ \frac{[\sum_{i,j}^{I,J} (\bar{C}_{ij} - \bar{C})A_j]^2}{(I \sum_{j}^{J} A_j^2)} \right\}^{1/2}. \tag{3}$$

Root-mean-square differences and correlations of area-weighted departures are used to compare the C2 and model total cloudiness. For example the root-mean-square differences (rmsd) of departures of annual means from the globally averaged annual mean are given by

$$\text{rmsd} = \left\{ \frac{[\sum_{i,j}^{I,J} (\bar{c}_{ij} - \overline{c2}_{ij})A_j]^2}{(I \sum_{j}^{J} A_j^2)} \right\}^{1/2}, \tag{4}$$

where $\bar{c}_{ij}$ is a departure of model or observed total cloudiness, and $\overline{c2}_{ij}$ is a departure of the C2 cloudiness. Note that the rmsds that will be used are based upon departures from their respective annual global or zonal means. Thus, differences in annual average global or zonal means between models, which might arise from varying definitions of total cloudiness, will not directly influence the rmsd values. Similarly, correlations of area-weighted departures of annual means are given by

$$r = \frac{(\sum_{i,j}^{I,J} \bar{c}_{ij}\overline{c2}_{ij}A_j^2)^{1/2}}{[\sum_{i,j}^{I,J} (\bar{c}_{ij}A_j)^2]^{1/2}[\sum_{i,j}^{I,J} (\overline{c2}_{ij}A_j)^2]^{1/2}}. \tag{5}$$

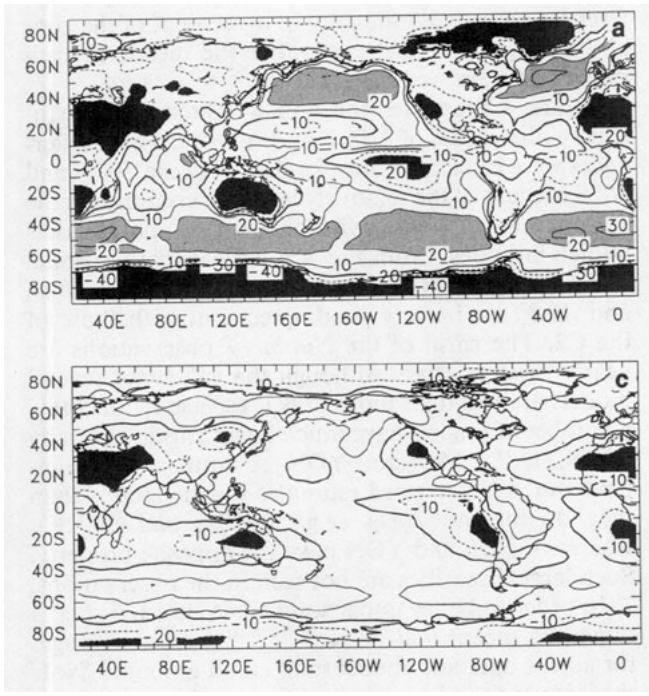

FIG. 3. Sample annual mean global cloudiness in percent minus global mean (Fig. 1a) for (a) the C2 observations, (b) the GLA model, and (c) the UCLA model. Contour intervals are 10%; zero lines are heavier; negative lines are dashed; regions with values greater than 20% have light shading; those with values less than −20% have heavy shading.

Again, using this definition the influences of differences in global or zonal means are minimized.

4. Annual means

Figure 1 shows the global area-weighted averages and standard deviations of annual mean total cloud amount for each of the models and observational datasets. In each case except for the *Nimbus-7* data these are for the common period July 1983 through June 1988. For the *Nimbus-7* they are for the 6 years of its record. The means of the C2 and Meteor observations are both near 62%, which is nearly 10% greater than that of the *Nimbus-7*. The model means tend to be near 55% but vary from a low of less than 28% for the SUNYANC model to a maximum of over 78% for the CSU model. The relatively large value for CSU partly may be due to the fact that it is one of the few models that do not incorporate a procedure for calculating fractional cloudiness. Most models have standard deviations from the global annual mean that are 5% to 10% smaller than the C2 and Meteor observations, suggesting much smaller spatial variability than observed. Only CSU has a value which is considerably larger. CNRM, GLA, JMA, and SUNYANC have standard deviations that are much smaller than any of the observations.

A more direct comparison of the observational and model results is the rmsd between the departures from the global means in the models and those in the observations. Figure 2 shows the globally averaged rmsd between the C2 annual mean total cloudiness at each 5° grid and those of the models and other datasets. This figure clearly shows that the spatial patterns of annual averages of the Meteor observations are in better agreement with those of the C2 observations than those of any of the models. However, UCLA has a rmsd that is comparable to that of N7. The largest rmsds are for those models that in Fig. 1b show the least spatial variability.

In order to better understand these statistics, Fig. 3 illustrates samples maps of the annual means of the C2 observations and the GLA and UCLA total cloudiness. The C2 observations illustrate most of the important known spatial variations in total cloud amount. The GLA simulation has much smaller spatial variability than the C2 observations. It also illustrates some clear differences, such as the minima over the eastern subtropical oceans and the maxima over the Northern Hemisphere high-latitude continents. The UCLA results exhibit larger spatial variability, which is more comparable with the observations, and fewer gross errors than the GLA model. Some of the improvement exhibited by the UCLA model may be related to the fact that it is one of the three models (with CSU and MRI) that has a prognostic planetary boundary-layer depth parameterization, which is designed to improve the prediction of marine stratus.

5. Seasonal cycle

Two different approaches are used to display and compare the mean seasonal cycle of total cloudiness. In the first differences between the zonal averages for the monthly means for two contrasting seasons (e.g., July minus January) are utilized. In the second a smoothed seasonal cycle is derived using the first two

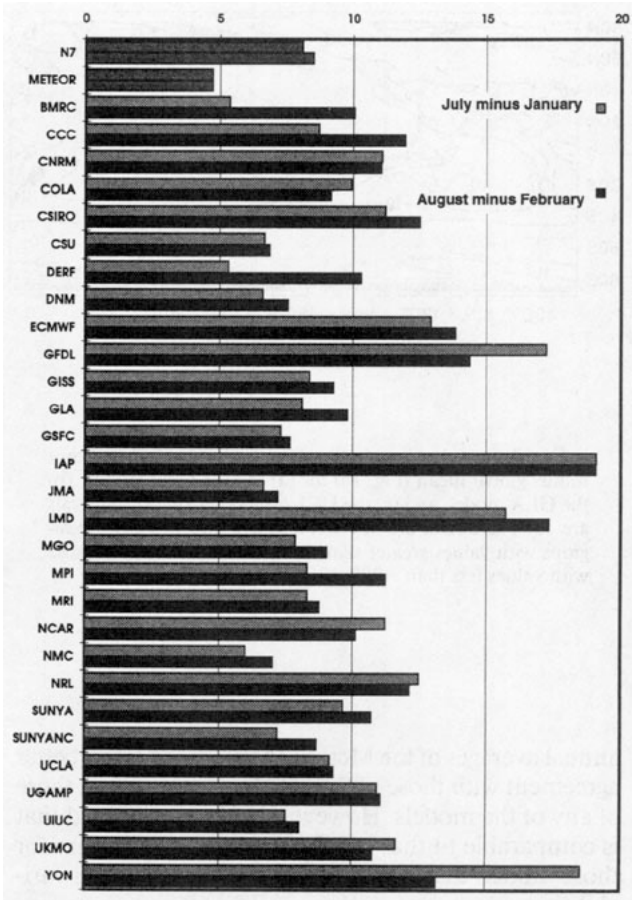

FIG. 4. Global area-weighted rmsd in percent between zonal mean total cloudiness of each model and data listed in Table 1 minus the values from the C2 analysis. July–January correspond to JmJ_j's departures, and August–February correspond to AmF_j's departures.

empirical orthogonal functions (EOFs) and associated time coefficients.

a. Zonal means

Long-term monthly mean zonally averaged cloud cover $\langle C_j^m \rangle$ is calculated for each observational and model dataset. In order to highlight the variations between opposite seasons, the differences between those zonal averages for different months are calculated. These zonal averages and differences for each calendar month and latitude are given by

$$\langle C_j^m \rangle = \sum_{y,i}^{Y,I} \frac{C_{ij}^{ym}}{(IY)}; \quad \langle C_j^{a-b} \rangle = \langle C_j^a \rangle - \langle C_j^b \rangle, \quad (6)$$

where a and b represent calendar months. For instance, the differences between July and January are given by $JmJ_j = \langle C_j^{\text{July–January}} \rangle$ and those for August and February by $AmF_j = \langle C_j^{\text{August–February}} \rangle$. Differences of these differences between the C2 estimates and those of each model or dataset then are calculated, for example, $\Delta JmJ_j = \langle C_j^{\text{July–January}} \rangle - \langle C2_j^{\text{July–January}} \rangle$. Those differences represent a measure of agreement of the zonally averaged seasonal cycle after the means of each dataset are removed.

Figure 4 illustrates the area-weighted root-mean-square differences of ΔJmJ_j and ΔAmF_j. These differences were calculated only for data between 70°N and 70°S because of the relatively large uncertainties in the seasonal cycles in the different observational datasets at high latitudes. From Fig. 4 it is clear that the zonal variations of the Meteor total cloudiness for both JmJ_j and AmF_j are in very good agreement with those of the C2. The rmsd of the *Nimbus-7* observations are nearly twice as large. Although the values for several models are less than those of N7, especially for JmJ_j, a number of models have much larger rmsd, especially GFDL, IAP, LMD, and YON. A number of models have much larger rmsd estimates for the AmF_js than they do for the JmJ_js (e.g., BMRC and DERF), whereas GFDL and YON have the opposite property. Such large disparities are not seen in the observations.

In order to better understand these statistics, Fig. 5 illustrates mean $JmJ_j = \langle C_j^{\text{July–January}} \rangle$ zonal averages for all the data and model total cloud amounts. Note there is very good agreement between the C2 and Meteor differences between about 70°N and 70°S, with large disagreements near the poles. The *Nimbus-7* differences are also similar to the other observations in the extrapolar regions except that the amplitude of the shifts in the Tropics is much larger. On the other hand, the values for nearly all of the models are fundamentally different from the C2 observations poleward of about 35°. Nearly all of the models underpredict summer cloudiness relative to winter in the midlatitudes of both hemispheres. This is evidenced by the fact that nearly all of the model values are less than the observations near 60°N and greater than the observations near 55°S. Most models also appear to underestimate the magnitude of the variations associated with the movement of the intertropical convergence zone (ITCZ). In addition for August–February (not shown), many models also shift the tropical maxima 5°–10° poleward of the observations. Thus, there is the strong suggestion that most models make substantial fundamental errors in the prediction of the seasonal cycle of cloudiness.

b. Smoothed seasonal cycle

In order to explore the model representations of the full spatial patterns of the seasonal cycle of total cloudiness, a smoothed seasonal cycle is produced for each model and observational dataset. This is done by calculating the EOFs of the departures of cloudiness from the long-term annual mean for all grids between 70°N and 70°S using the data for July 1983 through June 1988, except for the *Nimbus-7* observations, for which its entire period of record is used. The smoothed departure C_{ij}^{ym} at a given location and time is obtained

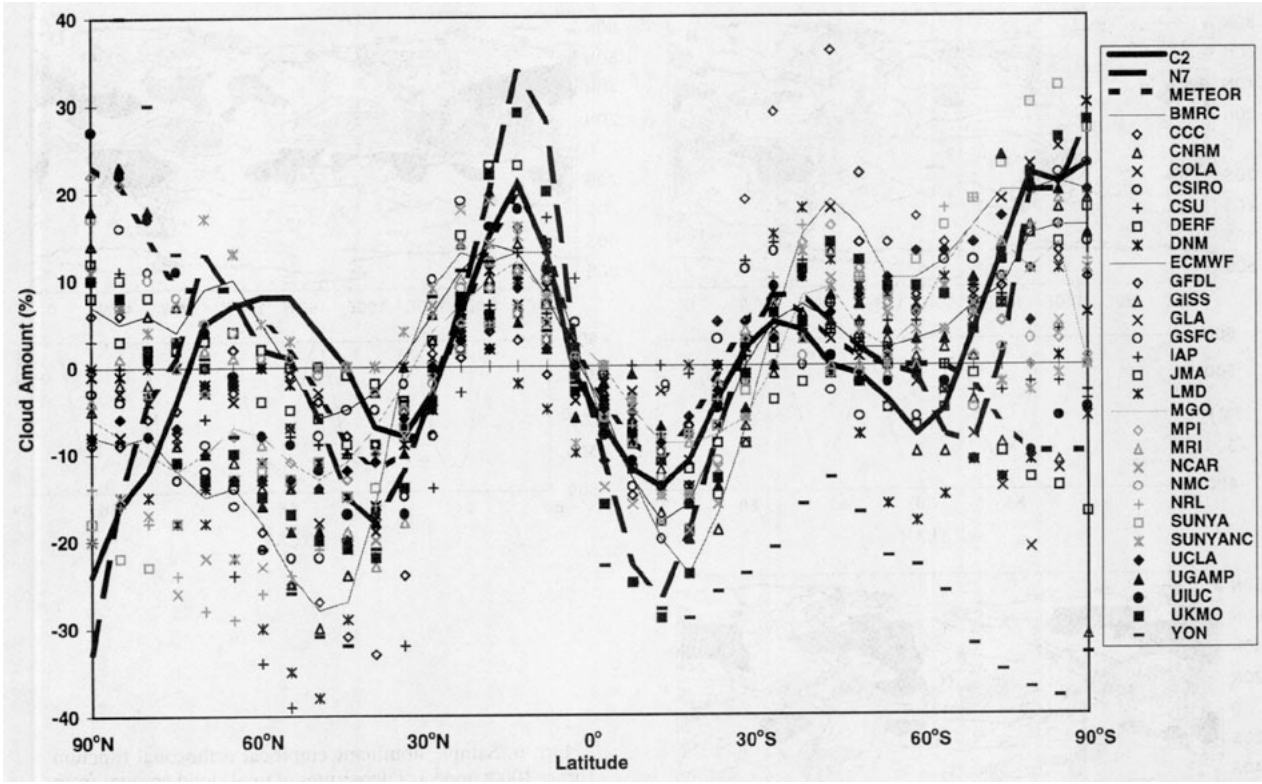

FIG. 5. July–January differences in zonal means of total cloud amount in percent for each of the models and datasets listed in Table 1.

from the two dominant seasonal EOFs (E^1 and E^2) and time coefficients (TC_1 and TC_2) such that

$$C_{ij}^{ym} = E_{ij}^1 TC_1^{ym} + E_{ij}^2 TC_2^{ym}. \quad (7)$$

These EOFs are calculated (Kutzbach 1967) using only data equatorward of 70° in order to avoid comparisons with the highly uncertain observational estimates near the poles. For all models and observations, the first two EOFs account for more than 50% of the total variance and meet the test of North et al. (1982) for separation of the eigenvalues.

Figure 6 illustrates samples of the leading EOFs for the C2 data and the UKMO and CSIRO models, which explain 38%, 43%, and 54% of the total variance, respectively. The C2 represents quite well the dominant EOFs of both the *Nimbus-7* and Meteor datasets. From Fig. 6 there is general agreement between the observations and models in the spatial patterns in the Tropics with, for instance, large maxima over Southeast Asia and Central America and minima over southern Africa, Australia, and the Amazon Basin. On the other hand the C2 observations appear to have considerably more regional-scale structure than do the model results. In addition, there is relatively large disagreement in the spatial patterns at the higher latitudes. All of the dominant EOF time coefficients show clearly the seasonal cycle. However, there is a fundamental difference between the C2 and CSIRO results in that the variations in CSIRO precede those of the observations by about 2 months.

In order to highlight the possible phase differences in the seasonal cycles, the 5-yr mean dominant EOF time coefficients for all of the models and observations are shown in Fig. 7. Before these values were plotted, care was taken to assure that the signs of the coefficients were such that positive signs correspond to maxima in cloudiness north of the equator. As expected, the observations and many of the models have maxima during July/August and minima during February. However, several models, indicated by bold names in the legend, have maxima and minima that lead the observations by about two months. Other models have coefficients with smaller but identifiable phase errors.

A comparison of the space–time variations of the smoothed seasonal cycle for all the models is summarized in Fig. 8. The rmsds (Fig. 8a) between the smoothed seasonal cycle of the C2 observations and those of the other observations show good agreement among the observations with rmsds less than 5.5%. Models, however, show rmsds of between about 7% and 14%. Figure 8b displays the correlations between the smoothed seasonal cycle of the C2 observations and other observations and model results. The correlations between the C2 and other observations are over 75%; those between the C2 and models are less than 62%. Several models stand out as having relatively

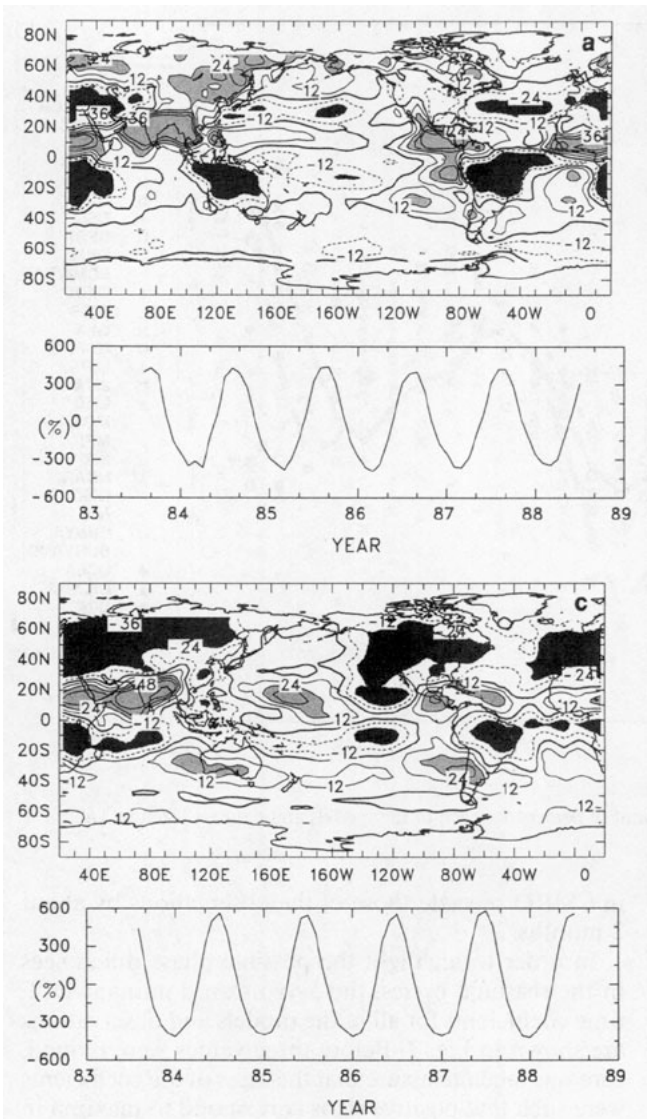

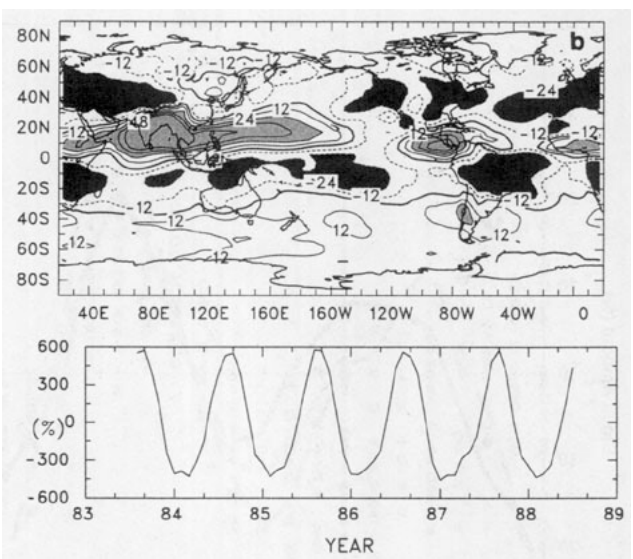

FIG. 6. Sample dominant empirical orthogonal function (times 1000; upper) of departures of total cloud amount from the annual means and associated time coefficients (lower) for (a) the C2 observations explaining 38% of the total variance, (b) the UKMO model explaining 43% of the variance, and (c) CSIRO model explaining 54% of the variance. Contour intervals are 12; zero lines are heavier; negative lines are dashed; regions with values greater than 24 have light shading; those with values less than −24 have heavy shading.

small correlations and large rmsds. Some of these have substantial errors in the phase of their seasonal cycles, as illustrated by Fig. 7. Other models, for example, GLA, IAP, LMD, and YON, do not exhibit large phase errors but still exhibit relatively large errors in simulating the seasonal cycle.

To better understand the possible reasons for the differences shown in Fig. 8, point by point rmsd were calculated between the smooth seasonal cycles of the C2 data and those of each of the models and the Meteor data for the period July 1983 through June 1988. Figure 9 illustrates those rmsd for the Meteor data and the UKMO and the CSIRO model results. Figure 9a shows that the rmsds between the C2 and Meteor observations are usually less than 6% with the largest differences in the monsoon regions of the Tropics and portions of the higher-latitude oceans. The rmsd between the C2 observations and the UKMO and the CSIRO model results (Figs. 9b,c) are greater than those in Fig. 9a. Figure 9, together with Fig. 6, suggests that the models are generally most successful at recreating the seasonal cycle of total cloudiness in the southern oceans. The largest differences in both models, which are not evident for the Meteor observations, occur over the high-latitude land areas of the Northern Hemisphere and the eastern oceans, where the models predict too little June–July–August cloudiness in both cases. On the other hand, the models both seem to overestimate the magnitude of the seasonal cloud variations in the region of the Asian Monsoon. A survey of similar maps for other models (not shown) suggests that these are all problem areas for most models. Errors in the eastern oceans and high-latitude land regions suggest the possibility that many models have problems in regions of stable planetary boundary layers. Those in the monsoon region, which are not evident along much of ITCZ

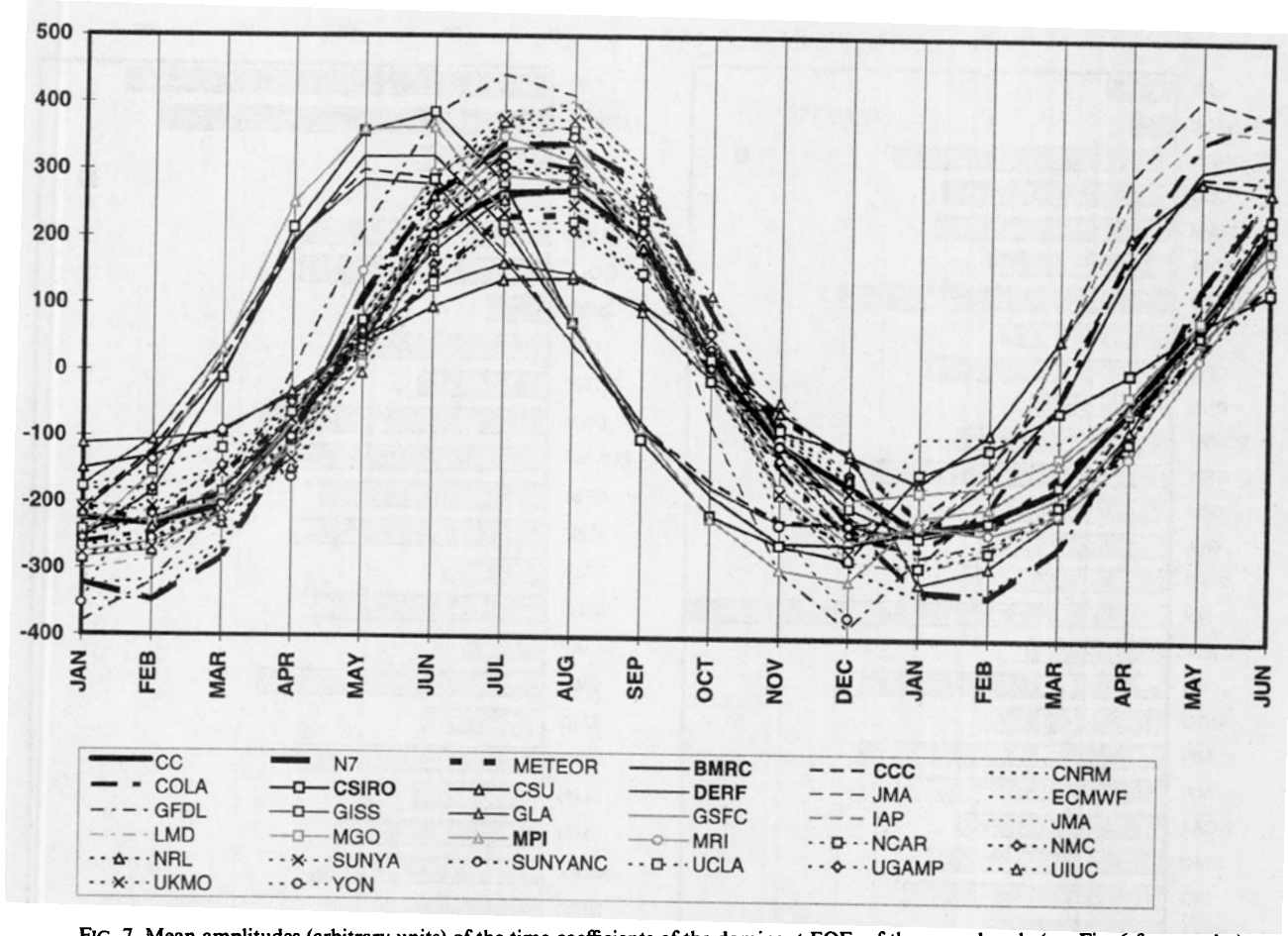

FIG. 7. Mean amplitudes (arbitrary units) of the time coefficients of the dominant EOFs of the annual cycle (see Fig. 6 for samples) for listed observations and models. Data for January through June have been repeated.

and South Pacific convergence zone, suggest more fundamental problems in modeling the Asian Monsoon.

6. Interannual variations

The ISCCP C2 observations for the period July 1983–June 1988 include only one significant large-scale climatic variation that can be associated with SST changes, the 1986/87 El Niño/Southern Oscillation (ENSO) event (Weare 1994). Figure 10 shows three examples for C2, CNRM, and ECMWF of the dominant EOFs of departures of total cloudiness from the 5-yr monthly means. All three results show spatial patterns dominated by the tropical Pacific Ocean and slow-changing time coefficients. The C2 observations illustrate the dominant changes in the central Equatorial Pacific found in previous observations (e.g., Philander 1990) with a broad peak found during 1986/87. The CNRM calculations show similar spatial features and a temporal peak slightly later in time. The ECMWF results show features indicative of more equatorial trapping than in C2 or CNRM and a temporal peak that slightly lags that of C2. Although the two dominant EOFs of C2 and most of the models meet the eigenvalue separation criterion of North et al. (1982), those of two models, GLA and IAP, did not and were excluded from further analysis.

From the interannual EOFs calculated for the C2 and Meteor observations and all of the models, smoothed interannual variations of total cloudiness were calculated from (7) based upon the two most important interannual EOFs. Figure 11 illustrates the area-weighted global mean correlations between the smoothed C2 variations and the other datasets. Correlations calculated over only the tropical domain are similar (Weare 1995). All of the correlations, including those with the Meteor observations, are less than 35%. The relatively small correlation with the Meteor observations is due to the fact that the dominant EOFs of the Meteor observations (not shown) fail to capture some of the well-known cloud changes in the tropical Pacific region. Many of the correlations, whose values have magnitudes less than about 15%, are clearly not significantly different from zero. Nevertheless, several models, including CNRM, ECMWF, LMD, and UKMO, show skill comparable to the agreement between the C2 and Meteor observations. The EOFs il-

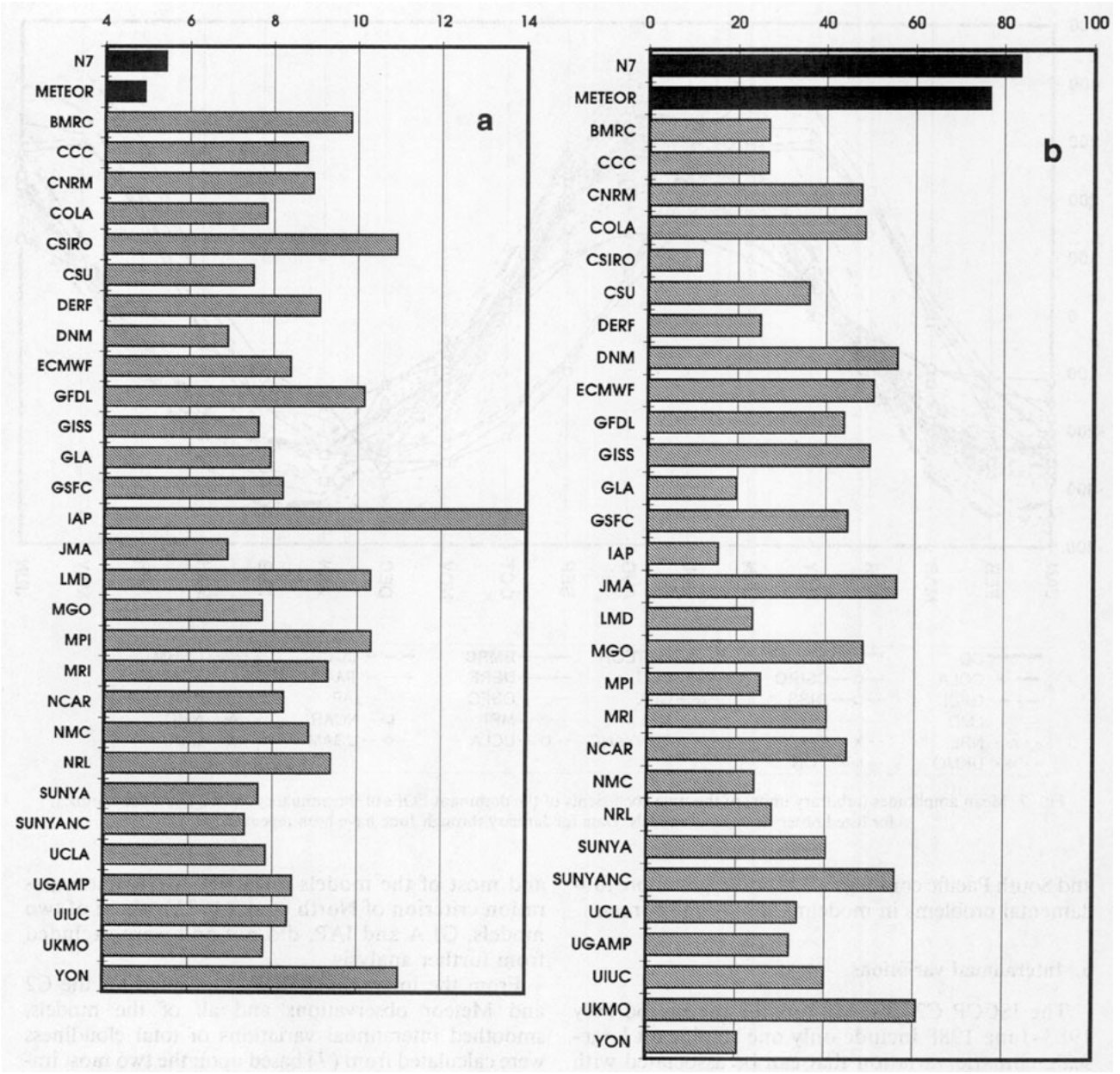

FIG. 8. Global area-weighted statistics comparing the smoothed seasonal cycles of the C2 data and the models and observations listed in Table 1. (a) Rmsd between the C2 estimates and other observations and models (percent) and (b) correlations between the C2 estimates and other observations and models (percent).

lustrated in Figs. 10b,c are typical of the more skillful models.

7. Discussion

Calculations of total cloudiness of 29 models participating in the Atmospheric Model Intercomparison Project are compared with the ISCCP C2, as well as with the *Nimbus-7* and Meteor observational estimates. Most models have global annual average total cloud amounts that are lower than the observations. However, this may not be significant because of differences in the definitions used for "total cloud amount." The root-mean-square differences between the annual means of the model calculations and the C2 observations after global means are removed are all greater than 14%. The largest rmsd are more than 28%, whereas the difference between the C2 and Meteor observations is less than 8%. The large rmsd in some cases are due to the fact that although a model qualitatively has spatial variations similar to those observations, the magnitude of those variations is much too small. In other

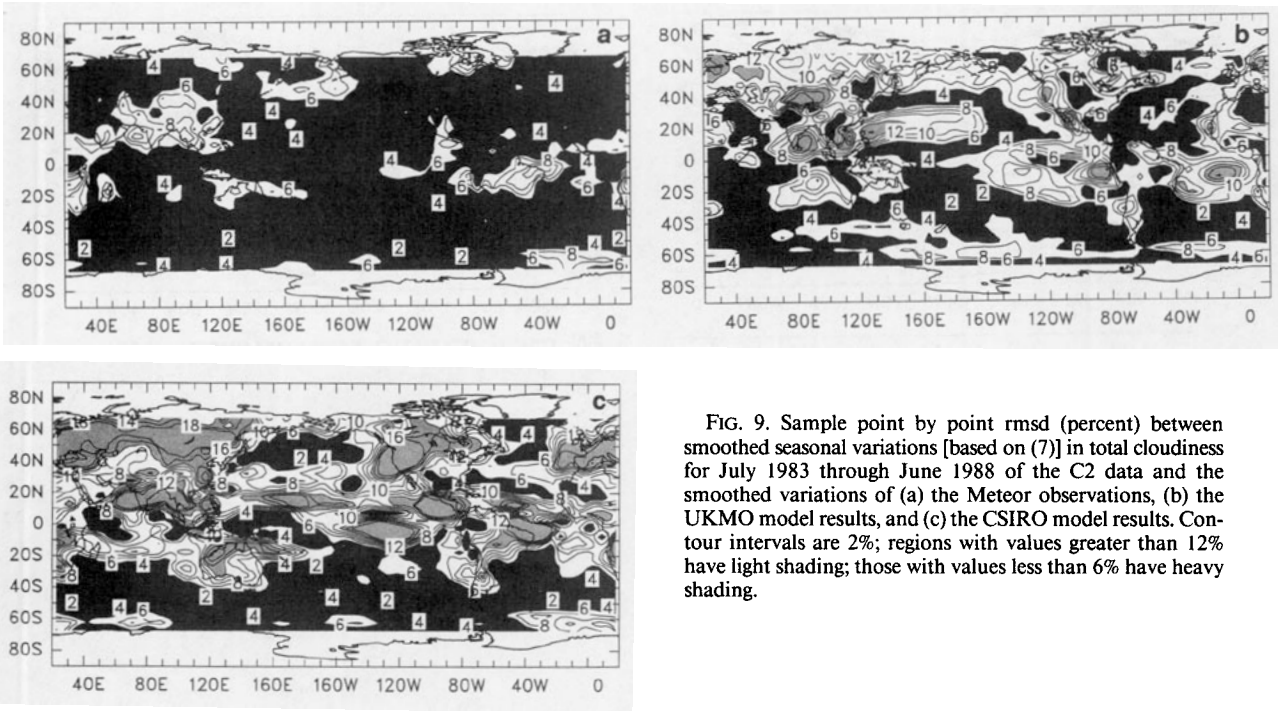

FIG. 9. Sample point by point rmsd (percent) between smoothed seasonal variations [based on (7)] in total cloudiness for July 1983 through June 1988 of the C2 data and the smoothed variations of (a) the Meteor observations, (b) the UKMO model results, and (c) the CSIRO model results. Contour intervals are 2%; regions with values greater than 12% have light shading; those with values less than 6% have heavy shading.

cases the models have produced the approximate magnitude of the spatial variability of the observations but display sizable errors in the pattern of that variability. These results suggest that all models need to make sizable improvements to adequately simulate even the geographic pattern of annual mean total cloudiness.

Not surprising, the deficiencies with respect to the model simulations of the mean seasonal cycle are also large, and the differences between models are more pronounced. For instance, the differences between the zonal averages of total cloudiness for contrasting seasons suggest that near 60° most models predict minima in cloudiness in summer, whereas observations strongly suggest the opposite. In addition some models appear to underestimate the magnitude and overestimate the latitudinal range of changes associated with the migration of the intertropical convergence zone, especially in the Northern Hemisphere. The smoothed seasonal cycle analyses suggest that a portion of these deficiencies in some models is the result of a simulated seasonal cycle that leads that of the observations by about two months. However, some models, which appear to have the proper phase of the seasonal cycle, still show large rsmd and small correlations when compared with the smoothed seasonal cycle of the C2 observations. No model in the AMIP experiment may be said to well-represent seasonal changes in total cloud amount.

The C2 and Meteor observations show a modest signal in total cloudiness for the only important interannual variation during the July 1983 through June 1988 observation period—the 1986/87 ENSO event. Many models fail to show any evidence of this event, whereas a few models reproduce it about as well as do the Meteor observations.

Although it is not the primary purpose of this study to identify which models are best at representing cloudiness, general conclusions are appropriate. CNRM, GLA, JMA, and SUNYANC seem to be somewhat less able than most models to replicate the observed spatial variations in the annual mean. Figure 12 is meant to summarize the relative effectiveness of each model in simulating the variations in C2 total cloud amount in three categories: the mean July minus January and August minus February differences of zonal averages from C2 (Fig. 4), the correlations with C2 of the smoothed seasonal cycle (Fig. 8b), and the correlations with C2 of the "smoothed ENSO" (Fig. 11). The bars in Fig. 12 are the relative ranks of the models, 1–29, from least to most able of reproducing the C2 observations. For instance, in Fig. 4 LMD has the largest difference and is assigned a rank of 1, NMC has the smallest difference from C2 and is assigned a rank of 29, and all other models are ranked in between. Likewise from Fig. 8b the largest correlation with C2 is for UKMO, which is assigned a 29, and from Fig. 11 the largest correlation is for ECMWF, which is again assigned a 29. Thus, in Fig. 12 the models with the longest bars are best able to reproduce this set of C2 observations and those with the shortest bars are least able. Most models fall in a range having a total rank between 30 and 50. However, a few models with values greater than 60 appear to be somewhat more able to reproduce the C2 variability, and a few with values less than 20 are less able to reproduce the observations.

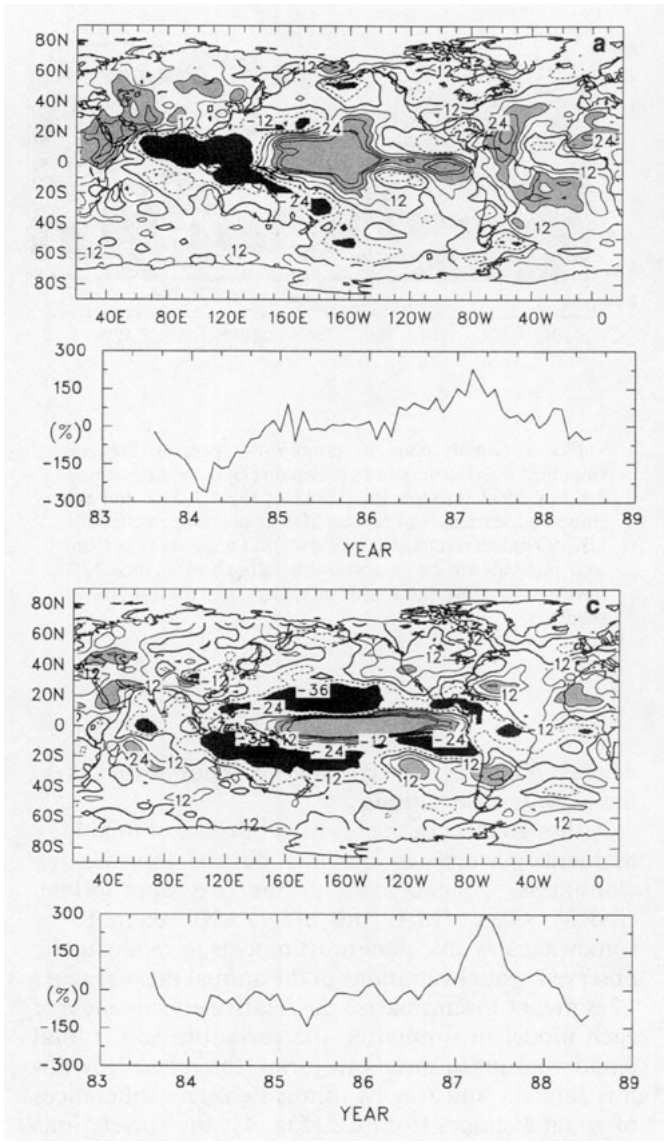

FIG. 10. Sample dominant empirical orthogonal function (times 1000; upper) of departures of total cloud amount from the 5-yr means and associated time coefficients (lower) for (a) the C2 observations explaining 11% of the total variance, (b) the CNRM model explaining 11% of the variance, and (c) the ECMWF model explaining 12% of the variance.

The information Fig. 12 and in Table 1 may be used to better understand why certain AMIP models are relatively good or poor at recreating the observed cloudiness variations. From Fig. 12 it is evident that models that better reproduce the ENSO results also tend to do well with seasonal variations. On the other hand, two models (DNM and MGO), which have high rankings for the two measures of the seasonal cycle, do relatively poorly in the "ENSO" comparison. This suggests that some models may be overly "tuned" to the observed seasonal cycle. Upon studying Table 1 to discern any possible consistent differences between models with ranks greater than 50 and less than 30 in Fig. 12, no distinctive patterns arise. The more successful models include both Kuo and Arakawa–Schubert convective parameterizations as do the less effective models. Likewise, both groups include a wide range of spatial resolutions and cloud fraction parameterizations. However, there is the general conclusion that models that have more sophisticated physical processes tend to better simulate the cloud observations.

Thus, although a primary aim of the Atmospheric Model Intercomparison Project is to identify the reasons why model outputs may differ from the observations and each other, there are major difficulties in establishing specific "causes" for the illustrated differences. These difficulties are in part related to the fact that the quality of a model's total cloudiness is a function not only of its cloudiness parameterizations but also its parameterizations of convection and boundary-layer processes and the overall quality of its large-scale dynamics. The identification of causes is also made more difficult by the fact that each modeling group has been forced to make a number of important, nearly arbitrary, decisions concerning the exact implementation of a convection or cloud fraction parameterization.

Partly in response to preliminary AMIP results, many of the illustrated models are undergoing substantial modifications and improvements to their parameterizations of physical processes. Thus, the statistics illustrated here may not be fully indicative of current model versions. Partly in response to preliminary reports of these and other AMIP comparisons and to anticipated improvements resulting from changes in model physics, AMIP soon will support a further suite of comparisons utilizing an extended 15-yr SST boundary condition dataset with updated models.

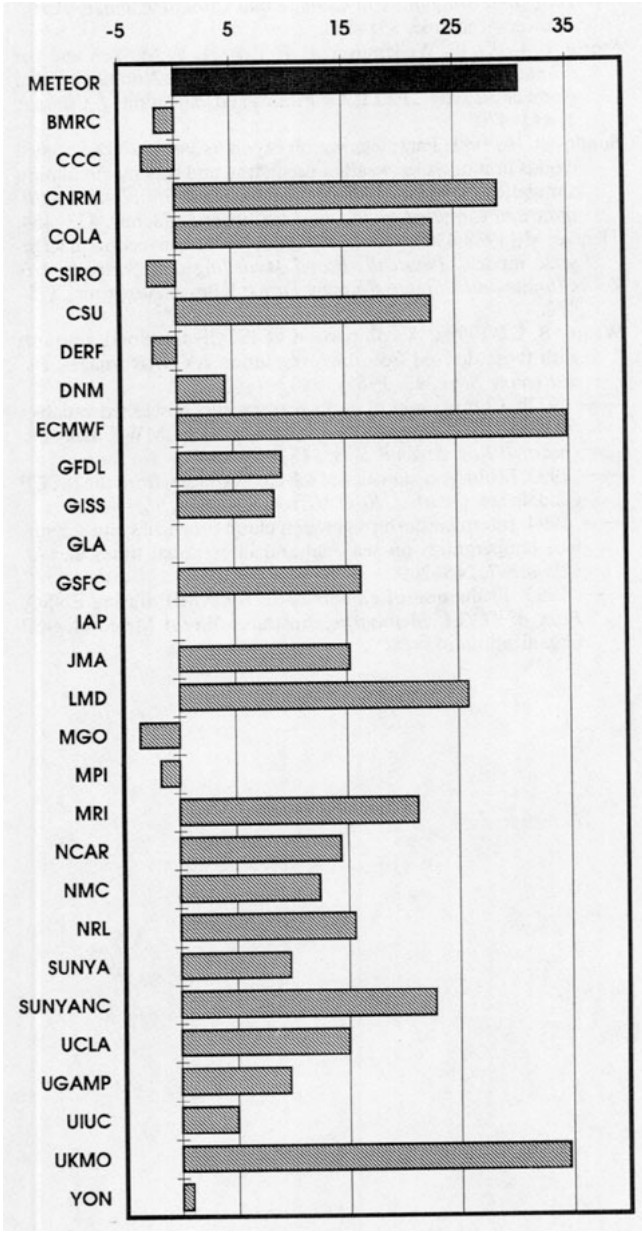

FIG. 11. Global area-weighted correlations (percent) comparing the smoothed "1986/87 ENSO event" (see Fig. 10) of the C2 data and those of the models and observations listed in Table 1.

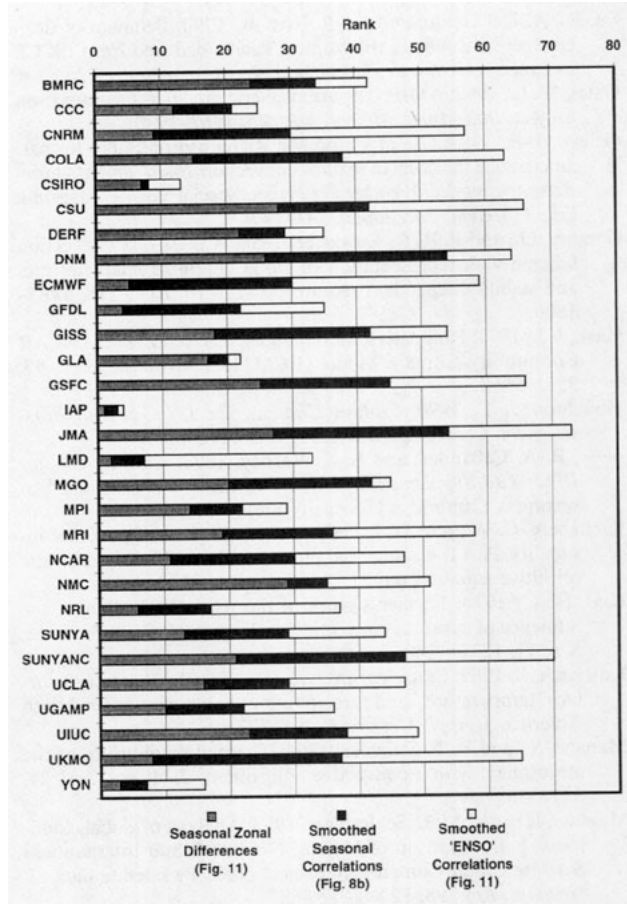

FIG. 12. Summed relative rank of each model in producing the C2 observations of seasonal differences in zonal averages (Fig. 4), the smooth seasonal cycle (Fig. 8b), and the "smoothed ENSO" (Fig. 11). As described in the text, the models with the longest columns are the most able and those with the shortest are the least able to reproduce the observations.

Acknowledgments. This work was support by the U.S. Department of Energy through the National Institute for Global Climatic Change and the Project for Climate Model Diagnostics and Intercomparison and the National Science Foundation. B.C.W. thanks Tomoniro Watanabe and Eric De Fonso for their help in retrieving and analyzing some of the AMIP results.

REFERENCES

Arakawa, A., and W. H. Schubert, 1974: Interaction of a cumulus cloud ensemble with the large-scale environment, Part I. *J. Atmos. Sci.*, **31**, 674–701.

Betts, A. K., and M. J. Miller, 1993: The Betts–Miller Scheme. *The Representation of Cumulus Convection in Numerical Models of the Atmosphere,* K. A. Emanuel and D. J. Raymond, Eds., Amer. Meteor. Soc., 107–121.

Bougeault, P., 1985: A simple parameterization of the large-scale effects of cumulus convection. *Mon. Wea. Rev.*, **113**, 2108–2121.

Del Genio, A. D., and M. S. Yao, 1988: Sensitivity of a global climate model to the specification of convective updraft and downdraft mass fluxes. *J. Atmos. Sci.*, **45**, 2641–2668.

Fu, R., A. Del Genio, and W. B. Rossow, 1990: Behavior of deep convective clouds in the tropical Pacific deduced from ISCCP radiances. *J. Climate,* **3,** 1129–1152.

Gates, W. L., 1992: AMIP: The atmospheric model intercomparison project. *Bull. Amer. Meteor. Soc.,* **73,** 1962–1970.

Geleyn, J.-F., 1987: Use of a modified Richardson number for parameterizing the effect of shallow convection. *Short- and Medium-Range Numerical Weather Prediction* (Special Vol.) T. Matsuno, Ed., *J. Meteor. Soc. Japan,* 141–149.

Gregory, D., and P. R. R. Rowntree, 1990: A mass flux convection scheme with representation of cloud ensemble characteristics and stability dependent closure. *Mon. Wea. Rev.,* **118,** 1483–1506.

Hack, J. J., 1994: Parameterization of moist convection *in* the NCAR Community Climate Model (CCM2). *J. Geophys. Res.,* **99,** 5551–5568.

Houghton, J. T., 1990: *Climate Change. The IPCC Scientific Assessment.* Cambridge University Press, 365 pp.

——, B. A. Callander, and S. K. Varney, 1992: *Climate Change 1992. The Supplementary Report to the IPCC Scientific Assessment.* Cambridge University Press, 200 pp.

Kreitzberg, C. W., and D. J. Perkey, 1976: Release of potential instability. Part I: A sequential plume model within a hydrostatic primitive equation model. *J. Atmos. Sci.,* **33,** 456–475.

Kuo, H. L., 1974: Further studies of the parameterization of the influence of cumulus convection on large-scale flow. *J. Atmos. Sci.,* **31,** 1232–1240.

Kutzbach, J., 1967: Empirical eigenvectors of sea-level pressure, surface temperature, and precipitation complexes over North America. *J. Appl. Meteor.,* **6,** 791–802.

Manabe, S., and R. F. Strickler, 1964: Thermal equilibrium of the atmosphere with a convective adjustment. *J. Atmos. Sci.,* **21,** 361–385.

Mokhov, I. I., and M. E. Schlesinger, 1993: Analysis of global cloudiness. 1. Comparison of Meteor, Nimbus 7, and International Satellite Cloud Climatology Project (ISCCP) satellite data. *J. Geophys. Res.,* **98,** 12 849–12 868.

——, and ——, 1994: Analysis of global cloudiness. 2. Comparison of ground-based and satellite-based cloud climatologies. *J. Geophys. Res.,* **99,** 17 045–17 065.

North, G. R., T. L. Bell, R. F. Cahalan, and F. J. Moeng, 1982: Sampling errors in estimation of empirical orthogonal functions. *Mon. Wea. Rev.,* **110,** 699–706.

Philander, S. G., 1990: *El Niño, La Niña, and the Southern Oscillation.* Academic Press, 289 pp.

Phillips, T. J., 1994: A summary documentation of the AMIP model. PCMDI Rep. No. 18, Program for Climate Model Diagnosis and Intercomparison, 343 pp.

Ramanathan, V., R. D. Cess, E. F. Harrison, P. Minnis, B. R. Barkstrom, E. Ahmad, and D. Hartmann, 1989: Cloud-radiative forcing and climate: Results from the Earth Radiation Budget Experiment. *Science,* **243,** 57–63.

Rossow, W. L., and R. A. Schiffer, 1991: ISCCP cloud data products. *Bull. Amer. Meteor. Soc.,* **72,** 2–21.

Smagorinsky, J., 1960: On the dynamical prediction of large-scale condensation by numerical methods. *Geophys. Monogr.,* No. 5, American Geophysical Union, 71–78.

Sommeria, G., 1988: Parameterization of the planetary boundary layer in large-scale atmospheric models. *Physically-Based Modelling and Simulation of Climate and Climate Change, Part I,* Kluwer Academic, 331–374.

Stowe, L. L., G. G. Wellemeyer, F. F. Eck, H. Y. M. Yeh and the *Nimbus-7* Cloud Data Processing Team, 1988: *Nimbus-7* global cloud climatology. Part I: Algorithms and validation. *J. Climate,* **1,** 445–470.

Sundqvist, H., 1988: Parameterization of condensation and associated clouds in models for weather prediction and general circulation simulation. *Physically-Based Modelling and Simulation of Climate and Climate Change, Part I,* Kluwer Academic, 433–464.

Tiedtke, M., 1988: Parameterization of cumulus convection in large-scale models. *Physically-Based Modelling and Simulation of Climate and Climate Change, Part I,* Kluwer Academic, 375–432.

Weare, B. C., 1992a: A comparison of ISCCP C1 cloud amounts with those derived from high resolution AVHRR images. *Int. J. Remote Sens.,* **13,** 1965–1980.

——, 1992b: Comparisons of multi-year statistics of selected variables from the COADS and the *Nimbus-7* and ECMWF data sets. *Quart. J. Roy. Meteor. Soc.,* **118,** 965–985.

——, 1993: Multi-year statistics of selected variables from the ISCCP C2 data set. *Quart. J. Roy. Meteor. Soc.,* **119,** 965–985.

——, 1994: Interrelationships between cloud properties and sea surface temperatures on seasonal and interannual timescales. *J. Climate,* **7,** 248–260.

——, 1995: Evaluation of cloudiness in the AMIP during ENSO. *Proc. of TOGA,* Melbourne, Australia. World Meteorological Organization, in press.